JOURNAL OF APPLIED CRYSTALLOGRAPHY
ISSN 1600-5767

Received 20 February 2023
Accepted 26 September 2023

Edited by V. T. Forsyth, Lund University, Sweden, and Keele University, United Kingdom

‡ These authors contributed equally to this work.

Keywords: small-angle X-ray scattering; SAXS; grazing-incidence X-ray off-specular scattering; GIXOS; asymmetric lipid bilayers; scattering length density; absolute SLD.

Supporting information: this article has supporting information at journals.iucr.org/j

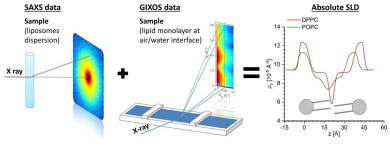

Absolute scattering length density profile of liposome bilayers obtained by SAXS combined with GIXOS: a tool to determine model biomembrane structure

Richard D. Harvey,[a]‡ Gianluca Bello,[b]‡ Alexey G. Kikhney,[c] Jaume Torres,[d] Wahyu Surya,[d] Christian Wölk[e]* and Chen Shen[f]*

[a]Division of Pharmaceutical Chemistry, Department of Pharmaceutical Sciences, University of Vienna, Josef-Holaubek-Platz 2, UZA 2, Vienna 1090, Austria, [b]Division of Pharmaceutical Technology and Biopharmaceutics, Department of Pharmaceutical Sciences, University of Vienna, Josef-Holaubek-Platz 2, UZA 2, Vienna 1090, Austria, [c]European Molecular Biology Laboratory, Hamburg Unit, c/o DESY, Building 25A, Notkestraße 85, 22607 Hamburg, Germany, [d]School of Biological Sciences, Nanyang Technological University, 50 Nanyang Avenue, Singapore 639798, Singapore, [e]Pharmaceutical Technology, Institute of Pharmacy, Medical Faculty, Leipzig University, Liebigstraße 20, Haus 4, 04103 Leipzig, Germany, and [f]Deutsches Elektronen-Synchrotron DESY, Notkestraße 85, 22607 Hamburg, Germany. *Correspondence e-mail: christian.woelk@medizin.uni-leipzig.de, chen.shen@desy.de

Lipid membranes play an essential role in biology, acting as host matrices for biomolecules like proteins and facilitating their functions. Their structures and structural responses to physiologically relevant interactions (*i.e.* with membrane proteins) provide key information for understanding biophysical mechanisms. Hence, there is a crucial need of methods to understand the effects of membrane host molecules on the lipid bilayer structure. Here, a purely experimental method is presented for obtaining the absolute scattering length density profile and the area per lipid of liposomal bilayers, by aiding the analysis of small-angle X-ray scattering (SAXS) data with the volume of bare headgroups obtained from grazing-incidence X-ray off-specular scattering (GIXOS) data of monolayers of the same model membrane lipid composition. The GIXOS data experimentally demonstrate that the variation of the bare headgroup volume upon change in lipid packing density is small enough to allow its usage as a reference value without knowing the lipid packing stage in a bilayer. This approach also has the advantage that the reference volume is obtained in the same aqueous environment as used for the model membrane bilayers. The validity of this method is demonstrated using several typical membrane compositions, as well as one example of a phospholipid membrane with an incorporated transmembrane peptide. This methodology allows us to obtain absolute scale rather than relative scale values using solely X-ray-based instrumentation, retaining a similar resolution to SAXS experiments. The method presented has high potential for understanding the structural effects of membrane proteins on the biomembrane structure.

1. Introduction

Lipid membranes are one of the structural foundations of living organisms. They support important biological activities by acting as hosting matrices for embedded transporters and signal transducing receptors, as well as facilitating endocytosis and secretory processes. Their structures and modifications exert fundamental influences on these processes, and thus structural information is essential for understanding underlying mechanisms.

Though numerous methodological developments have improved the resolution of protein and peptide structures, comparable advances on their lipid matrices are less frequently made (Zhang *et al.*, 1994; Petrache *et al.*, 1998;

Stefaniu *et al.*, 2014; Konarev *et al.*, 2021), despite the fact that this information is of high interest to understand biological processes which depend on membrane bending, stiffening and thickness modulation. Determining a high-resolution membrane structure under physiologically relevant conditions of milieu and lipid thermodynamics is equally important for understanding membrane biology at the molecular level.

Typical approaches in membrane studies use bilayer systems such as liposomes (Zhang *et al.*, 1994; Heftberger *et al.*, 2014; Konarev *et al.*, 2021; Kucerka, Tristram-Nagle *et al.*, 2005), hydrated supported multilayers (Kucerka, Liu *et al.*, 2005; Nagle, Cognet *et al.*, 2019; Scheu *et al.*, 2021; Kucerka, Tristram-Nagle *et al.*, 2005; Hristova & White, 1998), solid supported bilayers at bulk interfaces (Koutsioubas *et al.*, 2017; de Ghellinck *et al.*, 2015), or monolayers at air–water or oil–water interfaces (Stefaniu *et al.*, 2014). These models depict representative features of interest of more complex biological membranes, allowing high-resolution structures to be acquired by applying suitable X-ray or neutron scattering methods (Zhang *et al.*, 1994; Lyatskaya *et al.*, 2000; Heftberger *et al.*, 2014; Stefaniu *et al.*, 2014; Koutsioubas *et al.*, 2017; Konarev *et al.*, 2021; Kucerka, Tristram-Nagle *et al.*, 2005; Hristova & White, 1998). Among these methods, small-angle (X-ray) scattering (SAXS) studies on liposome dispersions of fully hydrated membranes are required to mimic biological settings. Such systems carry the advantage that the composition of the aqueous phase can be readily adjusted to model physiologically relevant conditions of pH, osmolarity, ionic strength or bulk ligand concentration.

SAXS data alone provide scattering length density (SLD) contrast profiles of phospholipid bilayers at sub-ångstrom resolution (Kucerka, Tristram-Nagle *et al.*, 2005) which clearly supply some structural information of the model membrane structure along the membrane normal, such as the distance between the high SLD phosphate groups of the two leaflets, the thickness of the lower SLD hydrocarbon core, and the shape of the headgroup toward the bulk and towards the core region [for an example, see Fig. 1(*a*)] (Konarev *et al.*, 2021; Petrache *et al.*, 1998). However, this is not sufficient to provide other physiologically important bilayer parameters such as area and volume per lipid or the hydration state of the headgroups. Obtaining these parameters requires an absolute SLD profile in reciprocal area units (*e.g.* $Å^{-2}$) to calculate the material density. Typically, SAXS data are obtained in arbitrary intensity units that reflect only the relative contrast variation from bulk solvent SLD. Measuring absolute SAXS intensity in reciprocal length units (*e.g.* cm^{-1}) with ±2% uncertainty requires accurate measurement of both transmission intensity and the exact number of scatterers in the volume illuminated by the X-rays (Franke *et al.*, 2017; Petrache *et al.*, 1998). This is difficult when the molarity of the sample suspension is not accurately known, or not homogenous with regards to the X-ray beam size or at high sample concentration (>5 mg ml^{-1}). One approach to solve the instrumental scaling is to use a heavy-atom label (*i.e.* bromine) in the hydrophobic core to alter the electron density contrast (Hristova & White, 1998), which demands that the label does not induce additional structural effects. An alternative approach is to use the bare headgroup volume, excluding hydration, obtained from membranes in the gel phase as a reference value for systems with the same headgroup, as this volume remains independent of the membrane phase (Petrache *et al.*, 1998; Klauda *et al.*, 2006). In addition, the lipid-specific volume of the SAXS sample was obtained in parallel with neutral buoyancy experiments (Wiener *et al.*, 1988; Petrache *et al.*, 1998; Kucerka, Tristram-Nagle *et al.*, 2005). Combining the two values yields the area per lipid and the scaling factor for the absolute SLD value. Later, simulation was also used to provide the specific volume of lipid in broader applications (Klauda *et al.*, 2006).

Following the same logic, we present a new alternative volumetric approach for obtaining absolute SLD profiles of liposomes, requiring input solely from complementary experimental X-ray data. Via the theoretical derivation, we

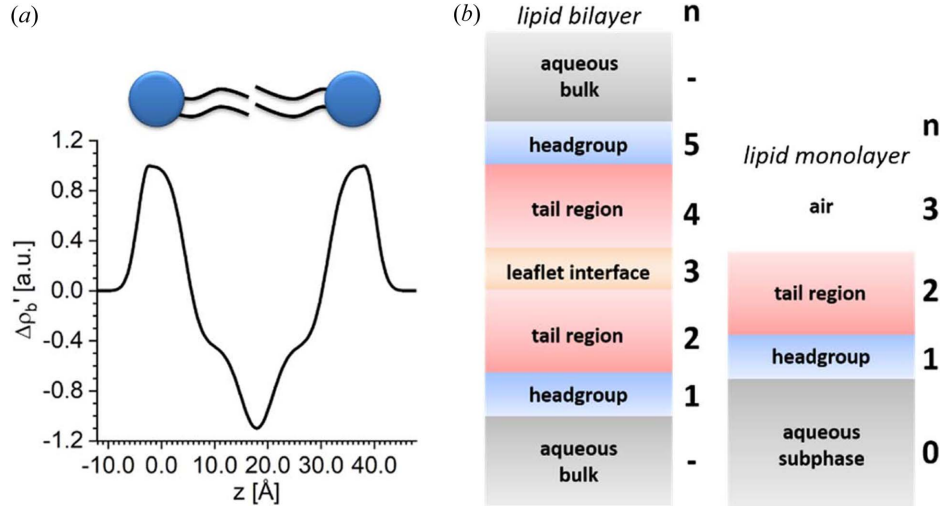

Figure 1
(*a*) Example of a relative SLD contrast profile of a lipid bilayer in liposomes obtained directly from a SAXS data analysis. Distances (z) are determinable, but the SLD contrast $\Delta\rho_b'$ is given in arbitrary units. Obtaining absolute SLDs is not possible. (*b*) Compartment models for a bilayer and for a monolayer.

show that the relative SLD contrast ratio within a lipid bilayer (hydrated head, tail) is sufficient to calculate the area per lipid and, accordingly, the absolute SLD profile once the volume of the bare headgroup is known. Moreover, we present the bare headgroup volume determined experimentally from monolayers of the same composition on the same aqueous bulk at various lateral pressures using grazing-incidence X-ray off-specular scattering (GIXOS) (Dai *et al.*, 2011). These GIXOS results demonstrate that variation of monolayer membrane phase and surface pressure has a negligible effect on the determination of the absolute SLD profile and area per molecule in the bilayer from SAXS analysis. It justifies the use of this value as the input reference to analyse bilayer data, regardless of the phase state of the lipids.

The method is validated by examples of commonly used phosphatidyl choline (PC) liposomes and PC/phosphatidyl serine (PS) binary mixed liposomes, all unextruded, to enable better comparability with previous results. In addition, we include a PC/PS membrane with embedded α-helical, envelope (E) protein from the severe acute respiratory syndrome coronavirus 2 (SARS-CoV-2), a protein that is assumed to induce membrane curvature during virion formation (Schoeman & Fielding, 2019). This peptide-embedded membrane requires modelling with an asymmetric bilayer profile, and thus it validates a broader application of this approach than simple model systems. The results presented demonstrate the applicability of the method to understand model biomembranes, also in the presence of interacting molecules such as proteins and peptides.

2. Materials and methods

2.1. Theory

Our approach to obtain absolute SLD profiles consists of three steps. (1) An arbitrary scale SLD contrast profile is obtained from vesicle dispersions from a conventional analysis of SAXS data (Kučerka *et al.*, 2006). (2) Langmuir monolayers of the same lipid composition and aqueous solvent are measured at different surface pressures by GIXOS, up to 0.9 Å^{-1} in Q_z, to obtain the monolayer absolute SLD profiles (Dai *et al.*, 2011). These monolayer SLD profiles provide the volume of the bare headgroup. (3) The absolute SLD profile of the bilayer is calculated from the SLD contrast profile using the bare headgroup volume as the reference. In this section, the theoretical derivation for obtaining the absolute SLD profiles is presented first, followed by the experimental examples in the next two sections.

2.1.1. Relative SLD contrast obtained from SAXS. The SAXS analysis we followed to obtain the arbitrarily scaled SLD profiles (Petrache *et al.*, 1998; Pabst *et al.*, 2003), though conventional, is briefly presented here for clarity. High-resolution analysis of the lipid bilayer structure from liposome suspensions requires the inclusion of at least three oscillations of a bilayer form factor, to roughly 0.6 Å^{-1} (Kučerka *et al.*, 2006). The scattering intensity of each sample in arbitrary scale is related to the membrane structure as

$$I(Q_r) = I_0 \frac{1}{Q_r^2} |F(Q_r)|^2 \int \mathrm{d}L\, P(L)\, S_L(Q_r) + I_{bkg}, \quad (1)$$

where the prefactor $1/Q_r^2$ is the Lorentz factor for bulk powder averaged geometry. I_0 and I_{bkg} are the arbitrary scaling factor and the background value. Q_r is the scattering vector length (Zhang *et al.*, 1994; Pabst *et al.*, 2003).

The bilayer form factor $F(Q_r)$ is the Fourier transformation of the bilayer SLD contrast $\Delta\rho_b'(z)$ against the bulk value $\rho_{b,water}$:

$$F(Q_r) = \int_{-D/2}^{D/2} \mathrm{d}z\, \exp(-iQ_r z)\, \Delta\rho_b'(z). \quad (2)$$

Here, a phospholipid bilayer is divided into five sub-compartments according to its SLD relative to the aqueous bulk [Fig. 1(*b*)]: the headgroup compartments of the two leaflets with $\Delta\rho_b'(z) > 0$, their hydrophobic tail compartments which have lower SLD than the headgroup regions and a region between the two leaflets with the lowest SLD (Nagle, Cognet *et al.*, 2019). The maximal excess SLD of the bilayer $\Delta\rho_{b,max}' = 1$.

Our test systems are unextruded liposome dispersions, either with lamellar orders that show Bragg peaks in the diffractogram or as uncorrelated bilayers without Bragg peaks. For lamellar phases, D is the repeat distance from the mid-point of the bulk on one side of the bilayer to the mid-point of the bulk on the other side. In the cases of uncorrelated bilayers, D is set to a number larger than the bilayer thickness (*e.g.* 100 Å). S_L and P are the structure factor of the lamellar structure of size L and the size distribution function, respectively. For an uncorrelated bilayer $S_L = 1$, $P(L) = 1$ for $L = 1$ and $P = 0$ for $L \neq 1$. For lamellae, the structure factor S_L of the bilayer structure of size L is

$$S_L(Q_r) = L + 2\sum_{n=1}^{L}(L-n)\cos(Q_r n D) \times \exp\left\{-(DQ_r/2\pi)^2\, \eta\left[\gamma + \ln(n\pi)\right]\right\}, \quad (3)$$

for the fluid phase of the multilamellar system (Zhang *et al.*, 1994; Pabst *et al.*, 2003), and γ is the Euler–Mascheroni constant. The Caille parameter η (Pabst *et al.*, 2003), following the Pabst *et al.* (2003) definition, accounts for the fluctuation of the bilayer sheet and its resulting loss of order (Zhang *et al.*, 1994). The normalized size distribution function $P(L)$ is given by

$$P(L) = \frac{1}{\int \exp(-L/L_0)\,\mathrm{d}L} \exp(-L/L_0), \quad (4)$$

with the width L_0 (Pabst *et al.*, 2003; Lyatskaya *et al.*, 2000).

2.1.2. General formula for obtaining absolute SLD profiles. The relative SLD difference $\Delta\rho_b'(z)$ is related to the contrast of the absolute SLD profile $\rho_b(z)$ from the bulk SLD $\rho_{b,water} = 9.42 \times 10^{-6}$ Å^{-2} by

$$\Delta\rho_b'(z) = \frac{\rho_b(z) - \rho_{b,water}}{f}, \quad (5)$$

with the normalization factor

$$f = \rho_{\mathrm{b,max}} - \rho_{\mathrm{b,water}}. \tag{6}$$

Here we show that it is possible to calculate this normalization factor using the physical constraint that the total scattering lengths of the hydrophobic core and hydrophilic head under the area $\hat{A}$ of one lipid are both known, and the same normalization factor value applies over all compartments of the membrane.

Initially, integration of $f\Delta\rho'_{\mathrm{b}}(z)$ over the lipid headgroup compartment or the hydrophobic core compartment is derived from the total scattering lengths, the volume of the compartment per lipid V_{head} and V_{tail}, and $\hat{A}$ as (Nagle & Wiener, 1989)

$$f\int_{\mathrm{bulk-head}}^{\mathrm{head-tail}} \Delta\rho'_{\mathrm{b}}(z)\,\mathrm{d}z = \frac{\sum_{\mathrm{head}} b - \rho_{\mathrm{b,water}} V_{\mathrm{head}}}{\hat{A}}, \tag{7}$$

$$f\int_{\mathrm{head-tail}}^{\mathrm{mid}} \Delta\rho'_{\mathrm{b}}(z)\,\mathrm{d}z = \frac{\sum_{\mathrm{tail}} b - \rho_{\mathrm{b,water}} V_{\mathrm{tail}}}{\hat{A}}. \tag{8}$$

The total scattering length of the headgroup region is the sum of the electron number of the atoms constituting the headgroup, the carbonyl–glycerol–phosphate (CGP) and the terminal groups (TER) such as choline (CHOL) or serine (SER), and hydration water (hydra):

$$\begin{aligned} &f\int_{\mathrm{bulk-head}}^{\mathrm{head-tail}} \Delta\rho'(z)\,\mathrm{d}z \\ &= \frac{\sum_{\mathrm{CGP}} b + \sum_{\mathrm{TER}} b + \sum_{\mathrm{hydra}} b - \rho_{\mathrm{b,water}}\left(V_{\mathrm{CGP}} + V_{\mathrm{TER}} + V_{\mathrm{hydra}}\right)}{\hat{A}} \\ &= \frac{\sum_{\mathrm{CGP}} b - \rho_{\mathrm{b,water}} V_{\mathrm{CGP}}}{\hat{A}}. \end{aligned} \tag{9}$$

This breakdown holds regardless of the SLD contrast since it only accounts for the number of electrons in the material. The TER contribution is cancelled with $\rho_{\mathrm{b,water}} V_{\mathrm{TER}}$ since its X-ray SLD is close to that of bulk water and is thus considered invisible (Nagle, Cognet *et al.*, 2019).

Dividing the head and the core equation yields the solution for the area per lipid $\hat{A}$ in the bilayer:

$$\frac{\int_{\mathrm{bulk-head}}^{\mathrm{head-tail}} \Delta\rho'_{\mathrm{b}}(z)\,\mathrm{d}z}{\int_{\mathrm{head-tail}}^{\mathrm{mid}} \Delta\rho'_{\mathrm{b}}(z)\,\mathrm{d}z} = \chi' = \frac{\sum_{\mathrm{CGP}} b - \rho_{\mathrm{b,water}} V_{\mathrm{CGP}}}{\sum_{\mathrm{tail}} b - \rho_{\mathrm{b,water}} D_{\mathrm{tail}} \hat{A}}, \tag{10}$$

$$\hat{A} = \frac{\chi' \sum_{\mathrm{tail}} b - \left(\sum_{\mathrm{CGP}} b - \rho_{\mathrm{b,water}} V_{\mathrm{CGP}}\right)}{\chi' D_{\mathrm{tail}} \rho_{\mathrm{b,water}}}. \tag{11}$$

D_{tail} is the thickness of one tail leaflet, measured from the head–tail interface to the middle plane of the leaflet interface within the bilayer. The normalization factor for the absolute SLD can be determined using the obtained $\hat{A}$ value as

$$f = \frac{\sum_{\mathrm{CGP}} b - \rho_{\mathrm{b,water}} V_{\mathrm{CGP}}}{\hat{A}\int_{\mathrm{bulk-head}}^{\mathrm{head-tail}} \Delta\rho'_{\mathrm{b}}(z)\,\mathrm{d}z} \tag{12}$$

using the SLD contrast of the headgroup region. With asymmetric bilayers, the scaling factors obtained from the two leaflets should be identical, within error. The absolute SLD thus can be obtained as

$$\rho_{\mathrm{b}}(z) = f\Delta\rho'_{\mathrm{b}}(z) + \rho_{\mathrm{b,water}}. \tag{13}$$

The value of f can equally be obtained from the contrast of the tail region as

$$f = \frac{\sum_{\mathrm{tail}} b - \rho_{\mathrm{b,water}} V_{\mathrm{tail}}}{\hat{A}\int_{\mathrm{head-tail}}^{\mathrm{mid}} \Delta\rho'_{\mathrm{b}}(z)\,\mathrm{d}z}, \tag{14}$$

where the tail volume $V_{\mathrm{tail}} = D_{\mathrm{tail}}\hat{A}$. The integration runs through the range of D_{tail}.

The calculation of $\hat{A}$ and f, via equations (11) and (12), demands a small enough variation of the volume V_{CGP} upon change of $\hat{A}$. A variation of ±5% in V_{CGP} is acceptable, since it only contributes an uncertainty of 5% to the scaling factor f. Considering a typical contrast between the maximal SLD of the headgroup of a bilayer and the aqueous bulk is $(12 \times 10^{-6}\ \text{Å}^{-2}) - (9.42 \times 10^{-6}\ \text{Å}^{-2}) \simeq 2.6 \times 10^{-6}\ \text{Å}^{-2}$ (Kucerka, Tristram-Nagle *et al.*, 2005; Nagle, Venable *et al.*, 2019), this 5% uncertainty corresponds to only $0.05 \times (2.6 \times 10^{-6}\ \text{Å}^{-2}) = 0.13 \times 10^{-6}\ \text{Å}^{-2}$ in the absolute SLD value. This variation has to be examined experimentally (Nagle, Venable *et al.*, 2019), although it was often assumed to be constant for the same type of headgroup (Petrache *et al.*, 1998).

2.1.3. Determination of reference headgroup volume from monolayers. Once the value of V_{CGP} is determined and proved to vary less than ±5%, the area $\hat{A}$ per lipid in the bilayer and the absolute SLD can be sequentially calculated from equations (11) and (12). The approach can be practically applied under this condition, without knowing the lateral pressure in the liposome membranes. This value and its variation can be experimentally obtained from GIXOS measurements (Dai *et al.*, 2011) using monolayers of identical lipid compositions on the same aqueous bulk, at various lateral pressures, through a conventional analysis described below (Dai *et al.*, 2011). In the next section we also show that the variation V_{CGP} is indeed within 5% for a specific headgroup type which allows it to be used in equations (11) and (12).

In a GIXOS measurement, the X-ray beam is incident at the air–buffer interface at ∼85% of the critical angle of the air–buffer interface, in order to enhance the monolayer scattering signal relative to the bulk scattering (Daillant & Alba, 2000). The GIXOS intensity is measured as a function of Q_z (*i.e.* the vertical Q component) up to 0.9 Å^{-1}, at $Q_{xy} \to 0\ \text{Å}^{-1}$. Aside from a constant background, the measured intensity $I(Q_z)$ consists of three contributions as

$$I(Q_z)\big|_{Q_{xy}\simeq 0} = I_0\, V_{\mathrm{f}}(\alpha_{\mathrm{f}})\left|\Phi(Q_z)\right|^2/\rho^2_{\mathrm{b,water}}, \tag{15}$$

where I_0 is an arbitrary scaling factor of the incoming flux (Daillant & Alba, 2000; Dai *et al.*, 2011). V_{f}, namely the Vineyard factor, is the subphase contribution (see Section S1 of the supporting information). It is a function of the critical angle of the air–buffer interface, the incident angle α_{i} and the scattering angle α_{f} (Dosch, 1987; Feidenhans'l, 1989).

The contribution from the interfacial layer $\Phi(Q_z)$ is a Fourier transformation of the gradient $\mathrm{d}\rho_\mathrm{b}(z)/\mathrm{d}z$ of the interfacial SLD profile $\rho_\mathrm{b}(z)$ for a monolayer on water at an arbitrary scale. However, the SLD values of the two sides, namely the superphase (air) and the subphase (water), are known to be 0 and ρ_water. Therefore, similarly to the reflectivity analysis, $\mathrm{d}\rho_\mathrm{b}(z)/\mathrm{d}z$ at an arbitrary scale corresponds to a unique SLD profile at absolute scale. $\mathrm{d}\rho_\mathrm{b}(z)/\mathrm{d}z$ and finally the absolute SLD were obtained by fitting the monolayer $I(Q_z)$ using a two-compartment model [Fig. 1(*b*)] (Als-Nielsen & Kjaer, 1989), consistent with the one leaflet of a bilayer model for SAXS: the CGP headgroup compartment with higher SLD $\rho_\mathrm{b,h,m}$ than the aqueous bulk ρ_water, and a tail compartment with lower SLD $\rho_\mathrm{b,t,m}$ than the headgroup region. The interfaces of headgroup–bulk, tail–headgroup and air–tail are all modelled by error functions (Als-Nielsen & Kjaer, 1989). The fitting of $I(Q_z)$ thus yields the thickness $D_\mathrm{t,m}$, $D_\mathrm{h,m}$ of the tail and the head compartments, their SLDs, and the width of the error functions describing the interfaces. The area per lipid

$$\hat{A}_\mathrm{m} = \sum_\mathrm{t} b/\left(\rho_\mathrm{b,t,m} D_\mathrm{t,m}\right) \tag{16}$$

in the monolayer is then calculated from the SLD and the thickness of the tail compartment, and the total scattering length $\sum_\mathrm{t} b$ of the two hydrocarbon tails of a lipid molecule. The latter

$$\sum_\mathrm{t} b = N_\mathrm{e,t} r_\mathrm{e}, \tag{17}$$

where $N_\mathrm{e,t}$ is the total electron numbers of two tails, *i.e.* 242e for DPPC and 265e for POPC, and

$$r_\mathrm{e} = 2.8 \times 10^{-15}\ \mathrm{m} \tag{18}$$

is the classical electron radius. The headgroup layer under this area contains a contribution from one CGP group. The rest of the volume has the SLD $\rho_\mathrm{b,water}$, contributed by the terminal group (choline/serine) and hydration water (Kučerka *et al.*, 2006). Therefore,

$$\begin{aligned} V_\mathrm{CGP} &= V_\mathrm{h,m} - \frac{\left(\rho_\mathrm{b,h,m} V_\mathrm{h,m} - \sum_\mathrm{CGP} b\right)}{\rho_\mathrm{b,water}} \\ &= \hat{A}_\mathrm{m} D_\mathrm{h,m} - \frac{\left(\rho_\mathrm{b,h,m} \hat{A}_\mathrm{m} D_\mathrm{h,m} - \sum\limits_\mathrm{CGP} b\right)}{\rho_\mathrm{b,water}}, \end{aligned} \tag{19}$$

where

$$\sum_\mathrm{CGP} b = 114 r_\mathrm{e}. \tag{20}$$

2.2. Experimental

2.2.1. Lipid stock solutions. 1,2-Dipalmitoyl-sn-*glycero*-3-phosphatidylcholine (DPPC), 1,2-dipalmitoyl-sn-*glycero*-3-phosphatidyl-L-serine (sodium salt, DPPS), 1-palmitoyl-2-oleoyl-PC (POPC) and POPS (sodium salt) were purchased from Avanti Polar Lipid as dry powders, and were dissolved in a mixture of chloroform/methanol (7:3 *v*/*v*, both from Merck KGaA) to yield four stock solutions at 1.5 m*M* lipid concentration. Stock solutions for binary lipid mixtures (PC:PS, 90/10 mol/mol) were obtained by mixing the PC and the PS stocks at a 90:10 volume ratio.

2.2.2. SARS-CoV-2 envelope protein purification and characterization. A SARS-CoV-2 E protein construct with N-terminal 6-His and MBP tags was derived from its SARS-CoV-1 counterpart by introducing T55S, V56F, E69R and G70del mutations by site-directed mutagenesis (Li *et al.*, 2014). A plasmid carrying this construct was transformed into *Escherichia coli* BL21-CodonPlus (DE3)-RIPL (Agilent). The cells were cultivated by the fed-batch method with K12 media 2 in a 1 l fermenter (Winpact) at 37°C. A 40% DO saturation was maintained by stirring, aeration and O_2 supplementation. Protein expression was induced with 0.5 m*M* IPTG at the same time feeding was started, and cultivation continued at 18°C overnight. The culture was harvested by centrifugation at 7500*g*. E protein was purified from the cell pellet by Ni–NTA chromatography and reverse-phase HPLC as described previously. The dry E protein (M_w = 8541.12 g mol^{-1}) powder was then dissolved in ethanol (denatured, ≥99.8%, Carl Roth GmbH) at 1 mg ml^{-1}.

2.2.3. SAXS experiment on liposome dispersion. Liposome dispersions for SAXS measurements contain ∼23 mg ml^{-1} of total lipid in 10 m*M* Tris buffer with 0.05 m*M* EDTA at pH 7.4 with and without 0.5 mol% E protein in the lipid mixtures. Buffer solutions were first prepared and adjusted to the required pH using concentrated hydrochloric acid. All buffer components were purchased from Merck KGaA. MilliQ water was provided at PETRA III (Hamburg, Germany). Lipid stock solutions of appropriate amounts were dried by rotary evaporation at 45°C, 25 mbar, for 45 min. Where needed, E protein ethanol stock solution was added to the lipid solution before drying in the rotary evaporator to a lipid:protein ratio of 200:1, equal to a 0.5 mol% of E protein in the lipid mixture. PO-lipid-containing samples were rehydrated at room temperature while DP-lipid-containing samples were rehydrated at 45°C to produce a final ∼23 mg ml^{-1} lipid dispersion.

SAXS experiments were performed in mail-in mode at the P12 BioSAXS beamline operated by EMBL at PETRA III (Hamburg, Germany) (Blanchet *et al.*, 2015) using a 0.2 × 0.12 mm (h × v) beam at 10.0 keV, with a Pilatus 6M detector (Dectris, Switzerland) at a distance of 3 m. Pure water and an empty capillary were measured at 22.3 and 37.0°C as the calibrants. Every liposome sample measurement of 10 × 0.1 s exposure was followed by at least two measurements on bare Tris buffer. All the data were first calibrated to the absolute scale (cm^{-1}) using the scaling factor calculated from the water data measured at the same temperature (Orthaber *et al.*, 2000). Background buffer data were subtracted from that of the liposome dispersions, which were then normalized by the lipid concentration. The data processing was performed with the automated pipeline *DATOP* with the *DATABSOLUTE* module at the beamline (Franke *et al.*, 2017).

2.2.4. GIXOS experiments on Langmuir monolayers. GIXOS experiments on Langmuir monolayers were

conducted at the Langmuir GID setup at the high-resolution diffraction beamline P08 at PETRA III (Hamburg, Germany) (Shen *et al.*, 2022; Seeck *et al.*, 2012). Lipid monolayers were directly prepared at the Langmuir trough (30 × 16 × 0.65 cm, Riegler and Kirstein GmbH, Germany) on the sample stage, which had been filled with buffer (10 m*M* Tris, 0.05 m*M* EDTA pH 7.4, 22.0°C). The 1.5 m*M* stock lipid solution was deposited dropwise using a gas-tight syringe (Hamilton Company, USA) to reach a total of 60 nmol of lipid at the surface, and then left for 15 min for solvent evaporation. Surface pressures of 35, 30 and 20 mN m^{-1} were achieved by a pre-compression to 38 mN m^{-1} and an expansion to the target value, both at 40 cm^2 min^{-1}. The GIXOS measurement started after the film had been relaxed at the target pressure for 15 min, while pressure was maintained and monitored; it was performed with a raw mode beam of 0.25 × 0.12 mm (h × v) at a 15 keV photon energy with an incident angle of 0.07° at the air–buffer interface, corresponding to 85% of its critical angle (Seeck *et al.*, 2012; Shen *et al.*, 2022). Two vertical slits of 0.25 and 1 mm widths were mounted 16 and 70 cm from the trough centre and offset horizontally such that only the scattered beam at 0.3° off-specular angle can pass, corresponding to $Q_{xy} \simeq 0.04$ Å^{-1} (Dai *et al.*, 2011). Intensity as a function of vertical scattering angle was acquired by a Pilatus 100k detector (Dectris, Switzerland) mounted after the second post-sample slit, with 6 × 20 s exposure time. Background scattering was suppressed by a vacuum beam path to the entrance window of the trough, a guard slit of 0.30 × 0.15 mm (h × v) at the entrance window, the helium atmosphere inside the trough case and the tungsten blade of the first post-sample slit which served as a beamstop. The vibration of the liquid surface was damped by placing a glass plate beneath the X-ray footprint area of the surface, which reduced the liquid depth to less than 1 mm (Als-Nielsen *et al.*, 1994). Data were reduced to $I(Q_z)$ with beamline-provided MATLAB-based tools.

2.2.5. SAXS and GIXOS data analysis. The fits of the SAXS and GIXOS data were performed with a purpose-built fitting toolbox using MATLAB. Their mathematics and a description of the monolayer two-compartment model are presented in Section 2.1. The mathematical expressions of the five-compartment model [Fig. 1(*b*)] for the bilayer SLD profiles can be found in Section S3 of the supporting information.

3. Results

The method described above was applied to liposomes of DPPC and POPC at 22°C, or two-component liposomes of DPPC with 10 mol% DPPS, and POPC with 10% POPS at

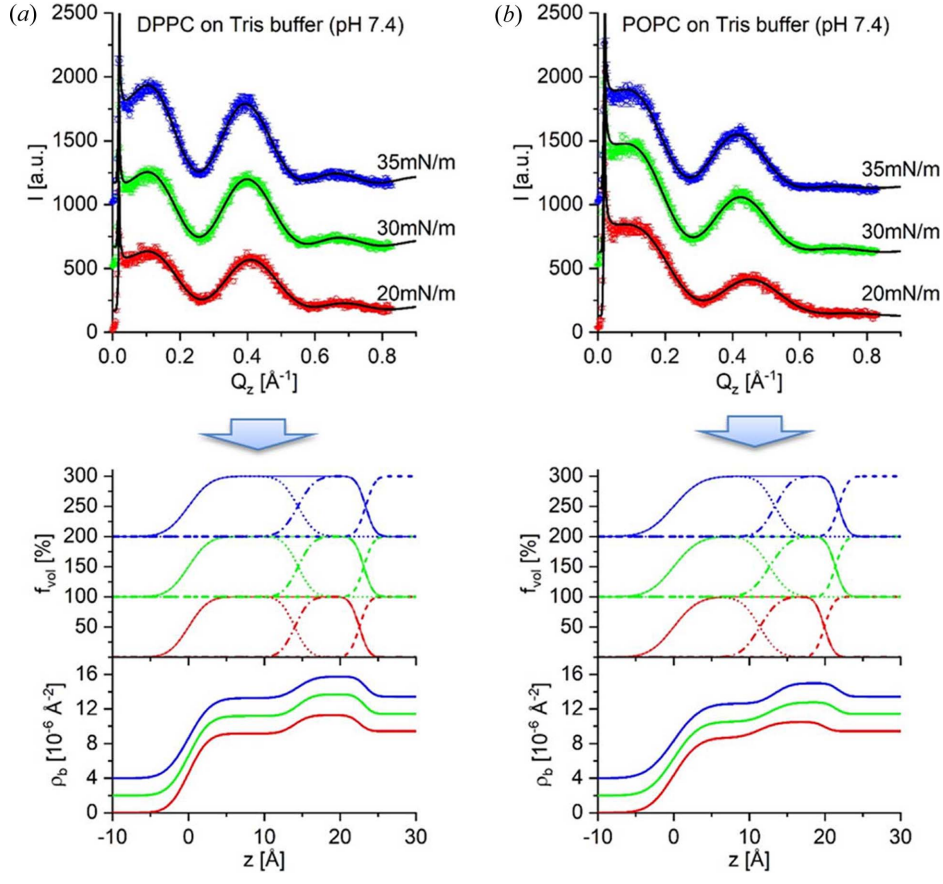

Figure 2
Fits (black lines) to GIXOS data (symbols) of (*a*) DPPC and (*b*) POPC monolayers at various surface pressures (offset by 500 and colour-coded), and the corresponding SLD profiles to the fits. The SLD profiles from different pressures are offset by 2 and colour-coded the same as the GIXOS data. Above the SLD profile is the volume occupation f_{vol} of the tail compartment as a dotted line, the headgroup compartment as a dot–dashed line, the sum of the two compartments as a solid line and the bulk water as a dashed line. They are offset by 100% and colour-coded.

Table 1
Structure parameters of DP and PO monolayers from the fitting of GIXOS data.

Fitting yields the thicknesses $D_{t,m}$ and $D_{h,m}$ of the tail and head compartments, respectively; their SLDs $\rho_{b,tm}$ and $\rho_{b,h,m}$; and the widths of the error functions $\sigma_{a/t,m}$, $\sigma_{t/h,m}$ and $\sigma_{h/w,m}$ for the air–tail, tail–headgroup and headgroup–water interfaces. V_{CGP} is the volume of the CGP group without hydration.

Monolayer	DPPC			POPC		
Π (mN m^{-1})	35	30	20	35	30	20
$\rho_{b,t,m}$ (10^{-6} Å^{-2})	9.26 ± 0.07	9.18 ± 0.06	9.16 ± 0.06	8.63 ± 0.07	8.53 ± 0.07	8.68 ± 0.07
$D_{t,m}$ (Å)	14.4 ± 0.6	14.5 ± 0.6	14.0 ± 0.5	13.4 ± 0.5	12.7 ± 0.5	11.4 ± 0.4
$\hat{A}_m$ (Å^2)	50.8 ± 2.2	51.0 ± 2.1	52.8 ± 1.9	64.3 ± 2.5	68.7 ± 2.8	75.1 ± 2.7
$V_{t,m}$ (Å^3)	732	738	741	861	870	855
$\rho_{b,h,m}$ (10^{-6} Å^{-2})	11.74 ± 0.05	11.68 ± 0.05	11.29 ± 0.02	10.98 ± 0.04	10.77 ± 0.03	10.50 ± 0.03
$D_{h,m}$ (Å)	8.9 ± 0.4	8.6 ± 0.4	8.5 ± 0.5	8.4 ± 0.4	8.7 ± 0.5	8.5 ± 0.5
V_{CGP} (Å^3)	226 ± 7	232 ± 7	249 ± 6	247 ± 6	251 ± 6	263 ± 5

Monolayer	DPPC:DPPS 90:10			POPC:POPS 90:10		
Π (mN m^{-1})	35	30	20	35	30	20
$\rho_{b,t,m}$ (10^{-6} Å^{-2})	9.00 ± 0.06	9.09 ± 0.07	9.04 ± 0.07	8.51 ± 0.07	8.60 ± 0.07	8.8 ± 0.1
$D_{t,m}$ (Å)	15.1 ± 0.6	14.9 ± 0.6	14.5 ± 0.6	12.8 ± 0.5	12.2 ± 0.5	11.4 ± 0.4
$\hat{A}_m$ (Å^2)	49.8 ± 2.0	50.0 ± 2.0	51.7 ± 2.2	68.2 ± 2.7	70.6 ± 2.9	74.0 ± 2.7
$V_{t,m}$ (Å^3)	753	746	750	872	863	841
$\rho_{b,h,m}$ (10^{-6} Å^{-2})	11.3 ± 0.1	11.24 ± 0.04	10.98 ± 0.04	10.83 ± 0.04	10.70 ± 0.03	10.50 ± 0.03
$D_{h,m}$ (Å)	9.1 ± 0.3	9.0 ± 0.4	8.8 ± 0.4	9.1 ± 0.5	8.9 ± 0.5	8.3 ± 0.5
V_{CGP} (Å^3)	248 ± 7	248 ± 6	260 ± 5	243 ± 7	250 ± 6	265 ± 5

37°C, all in 10 m*M* Tris, 0.05 m*M* EDTA at pH 7.4. In addition, we also applied the method to POPC/POPS (90:10) liposomes incorporating 0.5 mol% of the envelope (E) protein of SARS-CoV-2 in the same buffer conditions at 37°C. This example was chosen because it is part of our research activities and facilitates the development of the method described here. First, we will show that the reference volume of the CGP groups determined from GIXOS experiments on monolayers of the same composition and buffer varies less than 5% at different lateral pressures. This supports the use of the volume of this particular group in the SAXS analysis for bilayers. Then we will show the absolute SLD profiles of the lipid bilayers calculated using these reference values, and their consistency with previously published data (Pabst *et al.*, 2003; Kučerka *et al.*, 2006; Nagle, Cognet *et al.*, 2019).

3.1. Reference headgroup volume values of a typical phospholipid monolayer

Fig. 2 shows the fitted GIXOS data for PC monolayers at various pressures on Tris buffer, and their SLD profiles, consistent with literature values, *e.g.* with a headgroup peak SLD of ∼11.8 × 10^{-6} Å^{-2} and a tailgroup peak SLD of ∼8.7 × 10^{-6} Å^{-2} for condensed DPPC monolayers (Dyck *et al.*, 2005; Majewski & Stec, 2010). The parameters obtained for calculating V_{CGP} are compiled in Table 1, and the full set of parameters for all systems can be found in Figs. S1 and S2 and Table S1 of the supporting information. The average value of V_{CGP} for PC is almost constant at 245 ± 10 Å^3, and that for the 90:10 PC/PS headgroup is 252 ± 10 Å^3, with a variation of ±5% upon pressure change.

3.2. SLD profiles of exemplary lipid bilayers

The approach presented above was applied to finally obtain the bilayer SLD profile at absolute scale and the area per lipid in bilayers from the SAXS data of the five example systems (Fig. 3). Fitting with a bilayer compartment model [Fig. 1(*b*)] initially yields the relative SLD contrast profile $\Delta\rho'_b(z)$ (Fig. 3, inserts). The two datasets from PC-based liposome systems required the structure factor for ordered lamellae to fit the Bragg peaks and their diffuse scattering, and the three datasets from PC/PS binary liposomes were fitted with an uncorrelated bilayer model with S = 1. The complete set of parameters obtained is provided in Tables S2 and S3.

The $\Delta\rho'_b(z)$ of the gel DPPC bilayer and fluid POPC bilayer are consistent with literature profiles (Nagle, Cognet *et al.*, 2019; Klauda *et al.*, 2006; Heftberger *et al.*, 2014). The shapes of the two headgroup compartments at z = 0 Å are consistent with reported values (Nagle, Cognet *et al.*, 2019; Klauda *et al.*, 2006), with a steeper SLD drop towards the bulk and a shallower drop towards the core. The thickness D_c of the DPPC core region, measured as the distance between the two headgroup–tail interfaces, is 33.5 Å (Table 2), agreeing with the previously reported value of 34.2 Å (Nagle, Cognet *et al.*, 2019). The SLD values of the two tail leaflets are constant over ∼13 Å, being close to the bulk SLD ($\Delta\rho'_b \simeq 0$). These two leaflets are separated by a narrow SLD trough ($\Delta\rho'_{b,min} \simeq -1$), consistent with previous findings (Nagle, Cognet *et al.*, 2019). The core thickness D_c of 26.9 Å in the fluid POPC bilayer, and its lower SLD than the bulk, are also consistent with published data (Table 2) (Heftberger *et al.*, 2014). The interface between the two leaflets is wider and therefore less defined compared with the gel phase DPPC bilayer. The POPC/POPS (90/10) bilayer at 37°C has a similar structure to the POPC bilayer. However, the fitting of the data corresponding to the POPC/POPS bilayer with 0.5 mol% E protein required an asymmetric bilayer profile to account for the elevated SAXS intensity between 0.05 and 0.2 Å^{-1} [Fig. 3(*b*)] (Brzustowicz & Brunger, 2005; Semeraro *et al.*, 2021). Here, one bilayer leaflet

Table 2
Area ($\hat{A}$) per lipid in the two leaflets (index 1 and 2) of the liposome bilayers, the SLD normalization factor f calculated from the values of $\hat{A}$, and the corresponding volume V_{tail} of the tail region of the lipids.

The thickness D_c of the hydrophobic core, and the average values $\overline{\hat{A}}$ and $\overline{V_{tail}}$ of $\hat{A}$ and V_{tail} between the two leaflets, are also entered.

	22°C		37°C				
Membrane	DPPC	POPC	DPPC:DPPS 90:10		POPC:POPS 90:10	POPC:POPS 90:10 0.5% E	
V_{CGP} (Å^3)	242		248				
Leaflet index	1 and 2	1 and 2	1	2	1 and 2	1	2
$\hat{A}$ (Å^2)	45.5 ± 1.2	64.8 ± 1.5	49.0 ± 2.5	43.7 ± 1.6	64.3 ± 0.8	74.6 ± 3.7	58.3 ± 2.4
V_{tail} (Å^3)	763 ± 21	872 ± 24	803 ± 22	734 ± 16	874 ± 13	896 ± 32	842.8 ± 24
f	3.0 ± 0.1	1.88 ± 0.07	2.3 ± 0.1	2.4 ± 0.1	2.03 ± 0.06	1.7 ± 0.1	1.8 ± 0.1
D_c (Å)	33.5 ± 0.4	26.9 ± 0.4	33.2 ± 0.4		27.2 ± 0.2	26.5	
$\overline{\hat{A}}$ (Å^2)	45.5	64.8	46.3		64.3	66.4	
$\overline{V_{tail}}$ (Å^3)	763	872	768		874	869.3	

is thicker and has a higher SLD in both head and tail regions than the other. The data of DPPC/DPPS (90/10, 37°C) also require an asymmetric bilayer profile to provide reasonable fitting to the elevated SAXS intensity dips at ∼0.05 and 0.25 Å^{-1}. The SLD and thickness of the two chain leaflets are slightly different [Fig. 3(*b*) and Table 2].

The values of the headgroup area $\hat{A}$ and the tail region volume V_{tail} per lipid were initially calculated according to

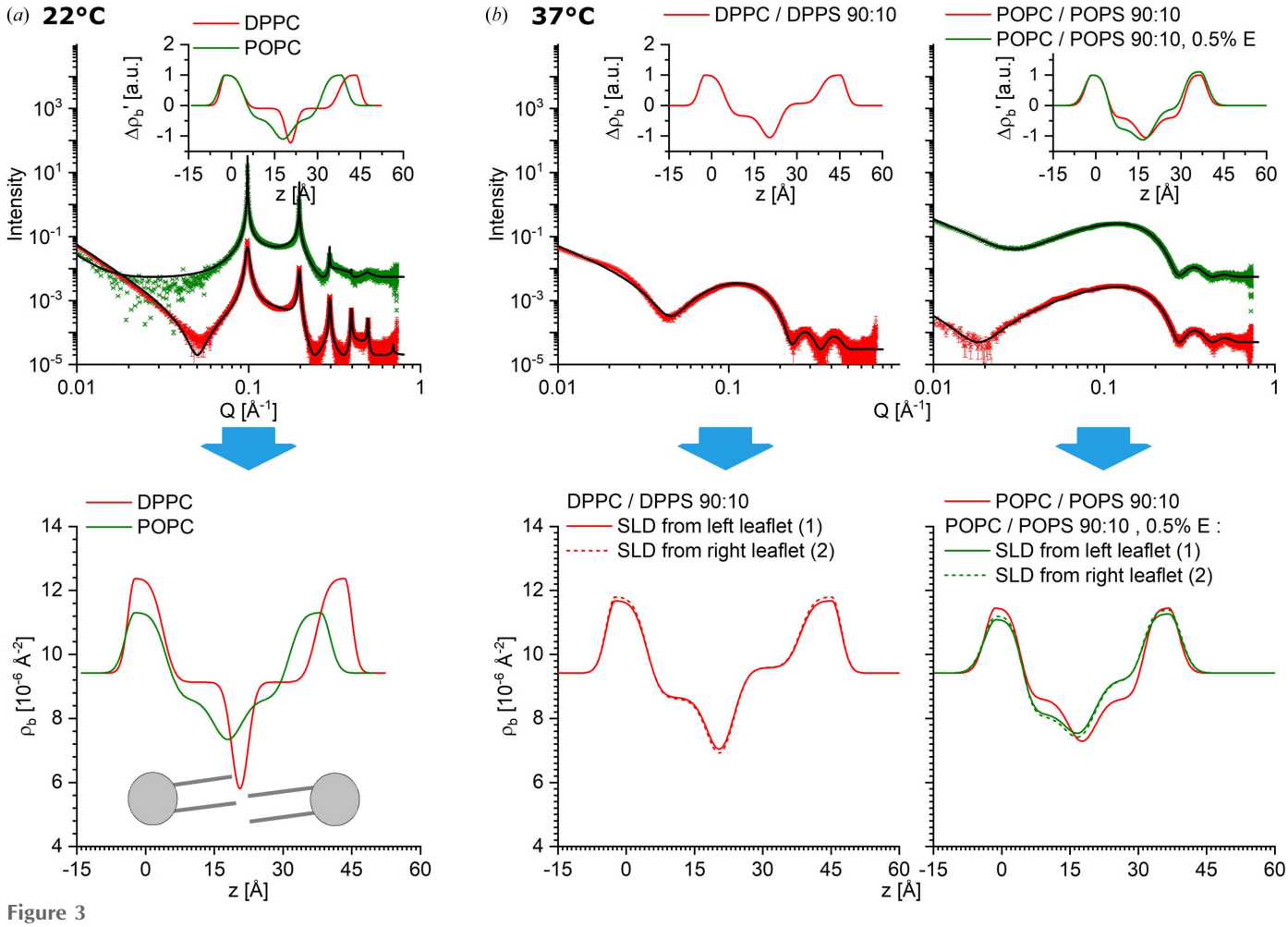

Figure 3
Fitted SAXS data (upper panel), SLD contrast profile (inset) and the absolute SLD profiles (lower panel) of (*a*) the two PC-based liposomes at 22°C, and of (*b*) the three PC/PS binary liposomes at 37°C. The data from the POPC/0.5% E liposome (own data, not published; incorporated E protein with a 200:1 lipid:protein molar ratio) and from the POPC/POPS (90/10) liposomes are shown in green and both are offset by 100. The SLD profiles from the two leaflets of the asymmetric bilayers are entered as different line types. The sketch of lipid molecules in the DPPC absolute SLD profile depicts the corresponding position of the headgroups, the tails and the interface between the two leaflets.

equation (11), with the input V_{CGP} values from GIXOS measurements (242 Å^3 for PC and 248 Å^3 for PC/PS), prior to the calculation of the normalization factor f for the absolute SLD. They were obtained for individual leaflets in the case of the asymmetric POPC/POPS/0.5% E protein and DPPC/DPPS bilayers. This method is applicable for the POPC/POPS/0.5% E protein bilayer since the compositional contribution of 0.5 mol% transmembrane protein to the bilayer SLD is negligible. In this regard, we included SLD simulations to support our claim in the supporting information. These values, together with those averaged between the two leaflets, are compiled in Table 2. The $\hat{A}$ values 45.5 and 64.8 Å^2 for the reference gel DPPC and fluid POPC bilayers (Table 2) are consistent with the literature (Heftberger *et al.*, 2014; Nagle, Cognet *et al.*, 2019; Kucerka, Tristram-Nagle *et al.*, 2005). The f values were then obtained by equation (12) using the contrast of the tail leaflet (Table 2) and were finally used to obtain the absolute SLD profile (Fig. 3, lower panels). In any of the asymmetric bilayers tested, the normalization factor values obtained from the two leaflets were identical (Table 2). Accordingly, a unique SLD profile was obtained independent of the choice of the leaflet (Fig. 3, lower panels: solid and dashed lines).

These examples validate our stepwise approach, by the agreement of the relative SLD contrast profiles and the values of core thickness and area per lipid with the literature, and the identical normalization factors obtained from the individual leaflets of one sample. Note that the fitting did not contain any constraint linking the contrast of the two leaflets.

4. Discussion

The intrinsic contrast variation of a lipid bilayer provides sufficient information to calculate an absolute SLD profile, once the value of the bare headgroup volume has been determined. This approach exploits the fact that the absolute SLD contrast of the headgroup and tail regions do not vary by the same factor when the area per lipid changes, due to the volume of water solvating the headgroup. The required volume of the bare headgroup can be experimentally determined from Langmuir monolayers by GIXOS measurements. Note that for X-rays it is the CGP part of the headgroup due to the similar SLD contrast between the terminal group (choline, serine *etc.*) and water. The choice of Langmuir monolayers allows the use of identical membrane compositions and subphase conditions at various lateral pressures. The GIXOS technique provides a low-background fast measurement that can approach the monolayer form factor (more than 0.9 Å^{-1} in Q_z), such that the bare headgroup volume can be obtained accurately. Moreover, this approach is also applicable to using X-ray reflectometry with more easily accessible and conventional laboratory sources.

The precondition to apply the headgroup volume value, in common with Petrache's approach, means that the dry volume of the headgroup is constant at different lateral pressures (Petrache *et al.*, 1998), since the lateral pressure in the bilayer is unknown. The experimental value obtained here varies by 5% between 20 and 35 mN m^{-1}, and between the fluid and the gel phase (Table 1). However, the impact of this variation is negligible as it only generates an uncertainty at 5% of the difference between the headgroup maximal SLD and the bulk water:

$$0.05\times\left[\left(12\times10^{-6}\ \text{Å}^{-2}\right)-\left(9.42\times10^{-6}\ \text{Å}^{-2}\right)\right]\simeq 0.1\times10^{-6}\ \text{Å}^{-2}.$$

Our five examples demonstrate the application of this method to both symmetric and asymmetric bilayers. The method was first validated by the literature-consistent values of area per lipid for the reference DPPC and POPC liposomes (Table 2) (Heftberger *et al.*, 2014; Nagle, Cognet *et al.*, 2019; Kucerka, Tristram-Nagle *et al.*, 2005). The theoretical derivation was further supported by the identical SLD profile obtained from the two different leaflets of the asymmetric bilayers (Fig. 3), without providing constraints that may couple the SLD of the two leaflets in SAXS fitting. We note that for the DPPC system the SLD scaling previously obtained is larger, which leads to a greater maximal SLD of the headgroup, up to 13.8 × 10^{-6} Å^{-2}, and a lower minimal SLD value down to 0.45 × 10^{-6} Å^{-2} (Heftberger *et al.*, 2014; Nagle, Cognet *et al.*, 2019; Klauda *et al.*, 2006). This apparent discrepancy can be attributed to the different CGP headgroup volumes applied, *i.e.* a recent value of 178 Å^3 for the gel phase DPPC (Nagle, Cognet *et al.*, 2019) and 213 Å^3 for the fluid DMPC and POPC (Klauda *et al.*, 2006; Heftberger *et al.*, 2014; Kucerka, Tristram-Nagle *et al.*, 2005), both obtained from simulations. Applying these two values to our calculation yields identical SLD profiles to theirs (Fig. S3), which further serves to validate our approach. Nevertheless, the volume of the bare headgroup may vary upon the change of physico-chemical conditions (Nagle, Venable *et al.*, 2019). We therefore recommend using experimentally determined volumes of the CGP group at the closest conditions possible, like in the method reported here. We are confident in using our values of 245 Å^3 for PC and 252 Å^3 for PC/PS (90:10), which were determined with the same lipid compositions in the same buffer, using monolayer SLD profiles consistent with data published from similar techniques (Dyck *et al.*, 2005; Bringezu *et al.*, 2007; Majewski & Stec, 2010; Ghosh *et al.*, 2012).

Moreover, the SLD profiles obtained provide an opportunity to investigate the relationship between a fully hydrated bilayer and an air–buffer interface monolayer. Fig. 4 shows a comparison between the liposome bilayer cross sections and those of their equivalent monolayers at 35 mN m^{-1} (22°C), which is considered to correspond to lateral pressure in a bilayer (Marsh, 1996; Watkins *et al.*, 2014). Although it is not possible to compile the SLD of a bilayer as the result of an imposition of two SLDs of a monolayer, it is interesting that the two fluid PO bilayers resemble the superimposed mirrored SLD profiles from two monolayers of the same lipid composition (Fig. 4, left), when their headgroup centroids are superimposed over those of the two bilayer headgroups. At this position, the CH_3-terminal interfaces of the two monolayer tail compartments are slightly separated at a distance of

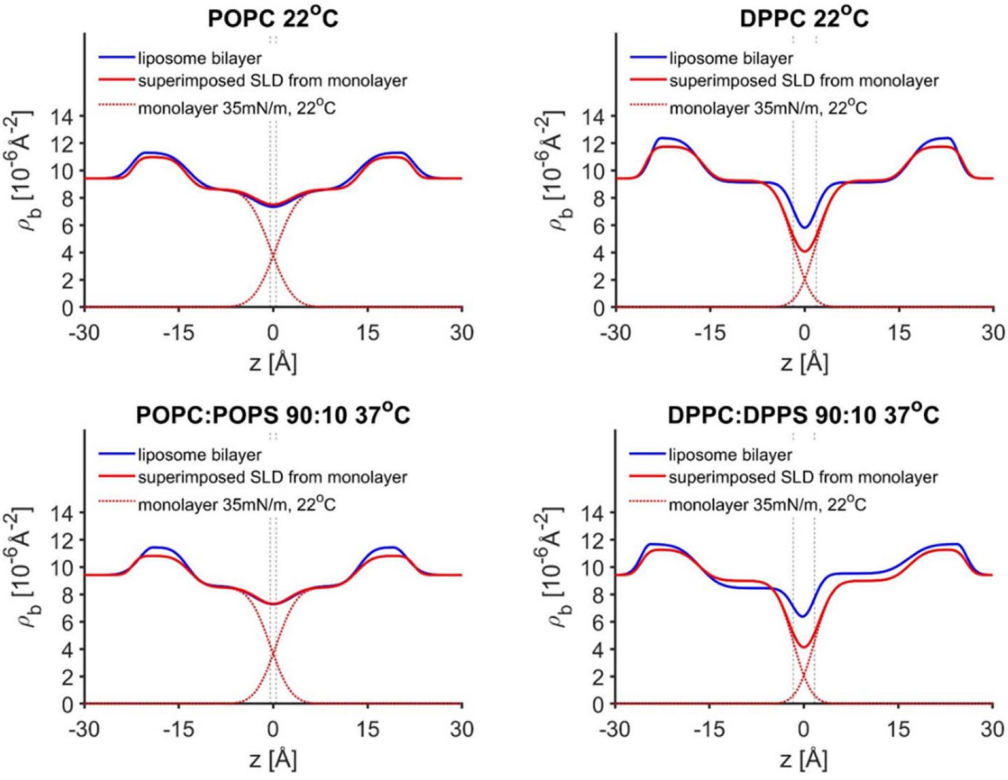

Figure 4
Absolute SLD profiles of the bilayers in liposomes versus the superimposed SLD profile from two mirrored monolayers of the same kind at 35 mN m^{-1}, 22°C. The monolayers are placed such that their headgroup centroids coincide with the centroids of the two bilayer headgroup compartments. The monolayer SLD profiles are also entered as dashed red lines. The resulting position of the CH_3-terminal interface of the monolayer tail region is depicted by a dashed vertical line.

0.9 Å (Fig. 4, vertical dashed lines). This separation mimics precisely the 'low SLD trough' as observed at the centre of the PO-liposome bilayers. A similar phenomenon was previously observed for myelin lipid membranes (Pusterla *et al.*, 2017). For the gel DP case, the superimposed SLD profiles qualitatively resemble the profile of the DP-liposome bilayers, although the details differ. Note that the superposition of two monolayers does not consider the bilayer asymmetry and we do not recommend using SLD profiles of monolayers to infer the SLD of a bilayer. Still, the headgroup compartments have a similar shape, width and SLD. The average SLD of the two tail compartments of the liposome bilayer is equal to the SLD of the monolayer tail region. However, superimposing the monolayer and bilayer headgroup centroids yields a larger separation of 3.8 Å between the CH_3-terminal interfaces of the DP monolayers, compared with the PO case. This larger separation is qualitatively consistent with the deeper 'SLD trough' between the DP leaflets. Thus, the experimentally observed trough is not as deep as the reconstructed one from mirror image monolayers, suggesting that the interface between the two bilayer leaflets is less defined than the monolayer tail–air interface. Aside from the direct observation we reported from our analysis, this discrepancy at the interfaces between monolayer and bilayer SLDs is further confirmation that structural data from monolayer studies need to be carefully considered when applied to a bilayer analysis. Also, for this reason, the method presented aims to theoretically and experimentally justify the reasoning behind the use of GIXOS as an aid to SAXS analyses.

5. Conclusions

In summary, we present a purely experimental approach with X-ray measurements to obtain the area per lipid and thus the absolute SLD profile of liposome membranes. Aside from the SAXS data, the only input required is the headgroup volume, which we suggest to measure under identical lipid composition and subphase conditions (*e.g.* from GIXOS or X-ray/neutron reflectometry experiments). The method is validated by selected reference phospholipid liposome systems. We also provide the full set of equations needed and the criteria of the data for such calculations. This approach is easily accessible as such measurements on Langmuir monolayers are routinely performed at major synchrotron (Mora *et al.*, 2004; Dai *et al.*, 2011) and neutron facilities as well as at laboratory X-ray instruments, and suitably high-quality solution SAXS experiments are achievable with both synchrotron and laboratory sources. Moreover, this approach is potentially applicable to more complex natural lipid membranes, in particular when lipid packing is affected by the aqueous environment.

6. Related literature

The following additional reference is cited in the supporting information: Vineyard *et al.* (1982).

Acknowledgements

We acknowledge DESY (Hamburg, Germany), a member of the Helmholtz Association HGF, for the provision of experimental facilities. Parts of this research were carried out at PETRA III and we would like to thank Dr F. Bertram and Mr R. Kirchhof for assistance in using beamline P08, and Dr M. Lippmann and Mrs A. Ciobanu for assistance in using the chemistry laboratory. Beam time was allocated for fast-track corona proposal P-20010207 and proposal H-20010161. The synchrotron SAXS data were collected on beamline P12 operated by EMBL Hamburg at PETRA III for the proposal SAXS-1095. CS thanks Professor B. Klösgen (SDU, Odense, Denmark), Professor J. F. Nagle and Professor S. Tristram-Nagle (CMU, Pittsburgh, USA) for the fruitful discussions on the structural analysis of lipid membranes. CS, GB, RDH and CW developed the methodology, performed the GIXOS experiments, prepared the samples for the SAXS experiments, analysed all the data, wrote the majority of the manuscript and conceptualized the research. CS also implemented the fitting procedure. AGK carried out the mail-in SAXS measurement at P12. JT and WS provided the SARS-CoV-2 E protein and the protocol to prepare the liposomes with the protein, and also contributed to the writing and conceptualization. Open access funding enabled and organized by Projekt DEAL.

Funding information

The research leading to this result has been supported by the project CALIPSOplus (grant No. 730872 awarded to DESY) from the EU Framework Programme for Research and Innovation HORIZON 2020. JT and WS thank the Singapore Ministry of Education for funding (Tier 1 thematic grant No. RT13/19). GB thanks the Galenus Foundation (AT) for the travel grant.

References

Als-Nielsen, J., Jacquemain, D., Kjaer, K., Leveiller, F., Lahav, M. & Leiserowitz, L. (1994). *Phys. Rep.* **246**, 252–313.
Als-Nielsen, J. & Kjaer, K. (1989). *The Proceedings of the NATO Advanced Study Institute*, pp. 113–138. New York: Plenum Press.
Blanchet, C. E., Spilotros, A., Schwemmer, F., Graewert, M. A., Kikhney, A., Jeffries, C. M., Franke, D., Mark, D., Zengerle, R., Cipriani, F., Fiedler, S., Roessle, M. & Svergun, D. I. (2015). *J. Appl. Cryst.* **48**, 431–443.
Bringezu, F., Majerowicz, M., Wen, S., Reuther, G., Tan, K.-T., Kuhlmann, J., Waldmann, H. & Huster, D. (2007). *Eur. Biophys. J.* **36**, 491–498.
Brzustowicz, M. R. & Brunger, A. T. (2005). *J. Appl. Cryst.* **38**, 126–131.
Dai, Y., Lin, B., Meron, M., Kim, K., Leahy, B. & Shpyrko, O. G. (2011). *J. Appl. Phys.* **110**, 102213.
Daillant, J. & Alba, M. (2000). *Rep. Prog. Phys.* **63**, 1725–1777.
Dosch, H. (1987). *Phys. Rev. B*, **35**, 2137–2143.
Dyck, M., Krüger, P. & Lösche, M. (2005). *Phys. Chem. Chem. Phys.* **7**, 150–156.
Feidenhans'l, R. (1989). *Surf. Sci. Rep.* **10**, 105–188.
Franke, D., Petoukhov, M. V., Konarev, P. V., Panjkovich, A., Tuukkanen, A., Mertens, H. D. T., Kikhney, A. G., Hajizadeh, N. R., Franklin, J. M., Jeffries, C. M. & Svergun, D. I. (2017). *J. Appl. Cryst.* **50**, 1212–1225.
Ghellinck, A. de, Shen, C., Fragneto, G. & Klösgen, B. (2015). *Colloids Surf. B Biointerfaces*, **134**, 65–72.
Ghosh, S. K., Castorph, S., Konovalov, O., Salditt, T., Jahn, R. & Holt, M. (2012). *Biophys. J.* **102**, 1394–1402.
Heftberger, P., Kollmitzer, B., Heberle, F. A., Pan, J., Rappolt, M., Amenitsch, H., Kučerka, N., Katsaras, J. & Pabst, G. (2014). *J. Appl. Cryst.* **47**, 173–180.
Hristova, K. & White, S. H. (1998). *Biophys. J.* **74**, 2419–2433.
Klauda, J. B., Kučerka, N., Brooks, B. R., Pastor, R. W. & Nagle, J. F. (2006). *Biophys. J.* **90**, 2796–2807.
Konarev, P. V., Gruzinov, A. Y., Mertens, H. D. T. & Svergun, D. I. (2021). *J. Appl. Cryst.* **54**, 169–179.
Koutsioubas, A., Appavou, M. S. & Lairez, D. (2017). *Langmuir*, **33**, 10598–10605.
Kučerka, N., Liu, Y. F., Chu, N. J., Petrache, H. I., Tristram-Nagle, S. T. & Nagle, J. F. (2005). *Biophys. J.* **88**, 2626–2637.
Kučerka, N., Tristram-Nagle, S. & Nagle, J. F. (2005). *J. Membr. Biol.* **208**, 193–202.
Kučerka, N., Tristram-Nagle, S. & Nagle, J. F. (2006). *Biophys. J.* **90**, L83–L85.
Li, Y., Surya, W., Claudine, S. & Torres, J. (2014). *J. Biol. Chem.* **289**, 12535–12549.
Lyatskaya, Y., Liu, Y. F., Tristram-Nagle, S., Katsaras, J. & Nagle, J. F. (2000). *Phys. Rev. E*, **63**, 011907.
Majewski, J. & Stec, B. (2010). *Eur. Biophys. J.* **39**, 1155–1165.
Marsh, D. (1996). *Biochim. Biophys. Acta*, **1286**, 183–223.
Mora, S., Daillant, J., Luzet, D. & Struth, B. (2004). *Europhys. Lett.* **66**, 694–700.
Nagle, J. F., Cognet, P., Dupuy, F. G. & Tristram-Nagle, S. (2019). *Chem. Phys. Lipids*, **218**, 168–177.
Nagle, J. F., Venable, R. M., Maroclo-Kemmerling, E., Tristram-Nagle, S., Harper, P. E. & Pastor, R. W. (2019). *J. Phys. Chem. B*, **123**, 2697–2709.
Nagle, J. F. & Wiener, M. C. (1989). *Biophys. J.* **55**, 309–313.
Orthaber, D., Bergmann, A. & Glatter, O. (2000). *J. Appl. Cryst.* **33**, 218–225.
Pabst, G., Koschuch, R., Pozo-Navas, B., Rappolt, M., Lohner, K. & Laggner, P. (2003). *J. Appl. Cryst.* **36**, 1378–1388.
Petrache, H. I., Tristram-Nagle, S. & Nagle, J. F. (1998). *Chem. Phys. Lipids*, **95**, 83–94.
Pusterla, J. M., Malfatti-Gasperini, A. A., Puentes-Martinez, X. E., Cavalcanti, L. P. & Oliveira, R. G. (2017). *Biochim. Biophys. Acta*, **1859**, 924–930.
Scheu, M., Komorowski, K., Shen, C. & Salditt, T. (2021). *Eur. Biophys. J.* **50**, 265–278.
Schoeman, D. & Fielding, B. C. (2019). *Virol. J.* **16**, 69.
Seeck, O. H., Deiter, C., Pflaum, K., Bertam, F., Beerlink, A., Franz, H., Horbach, J., Schulte-Schrepping, H., Murphy, B. M., Greve, M. & Magnussen, O. (2012). *J. Synchrotron Rad.* **19**, 30–38.
Semeraro, E. F., Marx, L., Frewein, M. P. K. & Pabst, G. (2021). *Soft Matter*, **17**, 222–232.
Shen, C., Kirchhof, R. & Bertram, F. (2022). *J. Phys. Conf. Ser.* **2380**, 012047.
Stefaniu, C., Brezesinski, G. & Möhwald, H. (2014). *Adv. Colloid Interface Sci.* **208**, 197–213.
Vineyard, G. H. (1982). *Phys. Rev. B*, **26**, 4146–4159.
Watkins, E. B., Miller, C. E., Liao, W. P. & Kuhl, T. L. (2014). *ACS Nano*, **8**, 3181–3191.
Wiener, M. C., Tristram-Nagle, S., Wilkinson, D. A., Campbell, L. E. & Nagle, J. F. (1988). *Biochim. Biophys. Acta*, **938**, 135–142.
Zhang, R. T., Suter, R. M. & Nagle, J. F. (1994). *Phys. Rev. E*, **50**, 5047–5060.